N O T I C E

THIS DOCUMENT HAS BEEN REPRODUCED FROM
MICROFICHE. ALTHOUGH IT IS RECOGNIZED THAT
CERTAIN PORTIONS ARE ILLEGIBLE, IT IS BEING RELEASED
IN THE INTEREST OF MAKING AVAILABLE AS MUCH
INFORMATION AS POSSIBLE

Evaluation of Inelastic Constitutive Models for Nonlinear Structural Analysis

Albert Kaufman
Lewis Research Center
Cleveland, Ohio

NASA

EVALUATION OF INELASTIC CONSTITUTIVE MODELS FOR

NONLINEAk STRUCTURAL ANALYSIS

Albert Kaufman

National Aeronautics and Space Administration
Lewis Research Center
Cleveland, Ohio 44135

ABSTRACT

The influence of inelastic materi.il models on computed stress-strain states, and therefore predicted lives, was studied for thermomechanically loaded structures. Nonlinear structural analyses were performed on a fatigue specimen which had been subjected to thermal cycling in fluidized beds and on a mechanically load-cycled benchmark notch specimen. Four incremental plasticity-creep models (isotropic, kinematic, combined isotropic-kinematic, combined plus transient creep) were exercised using the MARC program. Of the plasticity models, kinematic hardening gave results most consistent with experimental observations. Life predictions using the computed strain histories at the critical location with a Strainrange Partitioning approach considerably overpredicted the crack initiation life of the thermal fatigue specimen.

INTRODUCTION

Hot section components of aircraft gas turbine engines, such as combustor liners and turbine blades and vanes, are subject to progressive creep-fatigue damage resulting from cyclic thermomechanical loading under extreme gas pressure and temperature environments. A Strainrange Partitioning approach (ref. 1) to assess the durability of these components has been under development at the NASA Lewis Research Center. In order to apply this or similar methods, it is first necessary to determine the stress-strain-

temperature histoy of the part at the critical location where cracks will initiate.

As part of the life prediction studies at Lewis, wedge specimens have been thermally cycled in fluidized beds as described in reference 2. In these tests, two fluidized beds were used to rapidly heat and cool prismatic bar specimens of single or double edge wedge cross-section. Nonlinear structural analyses were performed for these specimens using the MARC program (ref. 3); the results are reported in references 4 and 5. These nonlinear analyses were for specimens of several alloys and used a combined isotropic-kinematic hardening model in MARC in conjunction with monotonic stress-strain properties taken from the literature.

Finite-element nonlinear analysis methods are becoming of increasing interest for computing the cyclic stress-strain response of hot section components (refs. 6 to 10). A major disadvantage of these methods, excessive computing costs, is being alleviated by advances in computer technology. Another deficiency is that current nonlinear analysis computer codes utilize classical constitutive material models whose accuracies vary with the type of material and the cyclic conditions involved. Furthermore, these classical models simplify the analyses by uncoupling time independent (plasticity) and time dependent (creep) effects, neglecting strain rate effects on plastic flow, and defining specific yield surfaces. The NASA Lewis Research Center has instituted programs to develop constitutive models which would more realistically represent the inelastic material behavior and be computationally practical for finite-element structural analysis. To verify the nonlinear structural analysis methodologies, Lewis is also sponsoring controlled cyclic experiments to provide strain data for benchmark notch specimens (ref. 11).

2

In this study existing constitutive models in the MARC computer program were exercised in inelastic analyses of an IN 100 wedge specimen subjected to thermal cycling and an Inconel 718 benchmark notch specimen subjected to mechanical load cycling. The objective of the study was to evaluate the effects on calculated hysteretic response, and therefore predicted life, of different inelastic constitutive models available in nonlinear analysis computer codes.

Three dimensional elastic and nonlinear structural analyses were performed on a thermally cycled double-edge wedge specimen. The nonlinear analyses were conducted using isotropic, kinematic and combined isotropic-kinematic hardening models and a combined hardening model in conjunction with a strain hardening creep law to account for cyclic time-dependent effects. Strain histories computed at the critical location from the different constitutive models were used in conjunction with the Strainrange Partitioning method to compare predicted lives against the observed crack initiation life. Two dimensional nonlinear analyses were performed for a mechanically load-cycled benchmark notch specimen; computed strain histories at the notch root using various material models were compared against measured notch strains.

PROBLEM DESCRIPTION

The primary structure considered in this study was an IN 100 alloy double-edge wedge specimen as illustrated in figure 1. Cracking was observed at the 1/4 span position on the leading edge after 38 cycles of testing in the fluidized bed facility (ref. 2).

The physical properties of the cast IN 100 alloy are presented in table I. Mean thermal coefficient of expansion data were converted to in-

3

stantaneous coefficients of thermal expansion for input into the MARC program. The modulus of elasticity was determined from monotonic stress-strain tests of tensile specimens. Cyclic stress-strain curves were obtained using the single specimen incremental step procedure and equipment described in reference 12. A typical cyclic stress-strain curve, with the loci of the curve tips represented by an exponential equation, is illustrated in figure 2. Also shown for comparison in figure 2 is a monotonic stress-strain curve represented by an exponential equation. Short-time cyclic creep tests were conducted on IN 100 specimens using the procedures and facilities described in reference 13. Preprocessor programs expressed both the cyclic stress-strain and creep data as functional relations in exponential form. These equations were incorporated into MARC by means of user subroutines. The constants of the cyclic and monotonic stress-strain equations are given in table II for various temperatures. In table III the constants of the cyclic creep equations are given for various temperatures.

The specimen was thermally cycled in fluidized beds maintained at 316° and 1088° C with an immersion time of 3 minutes in each bed. Transient temperature loading on the specimens was determined from thermocouple data as described in reference 2. Curve fits of thermocouple data along the mid-chord at the midspan at various increments after immersion into the fluidized beds are presented in figure 3. The temperature gradient through the thickness of the wedge was assumed to be negligible. Another set of thermocouple data was taken with thermocouples mounted along the leading edge over half the span to obtain the longitudinal (along the span of the specimen) temperature gradient for the different time increments.

Supplemental analyses to evaluate the constitutive material models were

4

also performed for a benchmark notch specimen of Inconel 718 alloy which was load cycled at a frequency of 0.167 Hz and a temperature maintained at 649° C. The material properties given in reference 11 were correlated in the same way as the IN 100 alloy properties.

ANALYTICAL PROCEDURE

Stress and total-plastic-creep strain distributions in the wedge specimens were calculated from the MARC nonlinear, finite-element computer program. Computations were performed for 34 time increments (17 heating, 17 cooling) into which the thermal cycle was subdivided, as shown in figure 3. The analyses were terminated when stable stress-strain hysteresis loops were obtained or after three cycles if the hysteresis loops remained unstable.

Plasticity computations were based on incremental plasticity theory using the von Mises yield criterion and normality flow rule. The yield surface under reversed loading was determined from the stress-strain properties and the selected hardening model. Three hardening models available in MARC (isotropic, kinematic and combined isotropic-kinematic) were selected for evaluation. Monotonic stress-strain properties were used in conjunction with the isotropic and combined models because of their initial instability. Saturated cyclic stress-strain properties were used for the stable kinematic model. A bilinear representation of the cyclic stress-strain curve, as shown in figure 2, was applied to the kinematic hardening model. The slope of the kinematic model was determined from energy considerations so that the strain energy, as indicated by the enclosed area, would be identical with that of the actual cyclic stress-strain curve. Creep effects during the cycle were considered for one case involving the combined model

5

by imposing four 30 second hold times during heating and two 6 second hold times at the start of the cooling part of the cycle. These intervals were selected because the combination of temperatures and stresses indicated a possibility of the occurrence of significant creep at these times in the thermal transient. The creep computations utilized the cyclic creep data in conjunction with a strain-hardening rule. A subroutine which was inserted into the MARC program in the form of yield strengths and work hardening slopes as functions of temperature, was used to determine the stress-strain propert'es for the local temperatures at the Gaussian integration points. Similarly the creep properties and laws were coded into another user subroutine which was used to obtain the creep strains at the integration points.

A preprocessor program converted the thermal loading data from the wedge specimen into the form of sixth-order polynomial equations. A subroutine, which was inserted into MARC, interpolated from these equations for the local temperatures at the Gaussian integration points.

The finite element model for the wedge specimen is illustrated in figure 4. Because of symmetry only one-fourth of the specimen needed to be modelled; this model was bounded by the surface and intersecting midchord and midspan planes of symmetry. The element used was a 20 node, isoparametric, three dimensional block with 8 corner nodes and 12 edge midpoint nodes. This element had 27 Gaussian integration points. The model consisted of 36 elements with a total of 315 nodes and 778 unsuppressed degrees of freedom.

All nodes initially on the midspan and midchord faces of the model were constrained to lie on the midspan and midchord planes respectively. In addition, one node at the leading edge was constrained chordwise (leading to trailing edge) in order to prevent rigid body motion in that direction.

The analytical procedure used for the benchmark notch specimen was basically the same as for the wedge specimen. Each cycle was subdivided into 30 load steps. One fourth of the specimen was modelled as shown in figure 5 using 592 plane strain, triangular elements with a total of 335 nodes.

RESULTS AND DISCUSSION

The critical location for crack initiation in the thermally cycled double-edge wedge specimen is at the leading edge at a quarter of the specimen span from either end. Results of both elastic and inelastic structural analyses determined that the critical location based on the region of the finite element model with the largest total strain range during the cycle was coincident with the observed crack initiation site. In the following discussion, the stress-strain results for the critical location were actually computed at the closest Gaussian integration point which was 0.056 centimeter from the surface at the quarter span.

The stress-total strain solutions at the critical location from the MARC elastic and nonlinear analyses of the wedge specimen are shown in figure 6. All stresses and strains in this figure were effective or equivalent values which were originally computed as positive numbers. However, in order to construct stress-strain hysteresis loops for life prediction purposes, the stresses and total strains were assigned positive or negative signs depending on the signs of the highest magnitude principal stresses or strains. Nonlinear stress-strain hysteresis loops are presented for the second cycle of the analyses. During heating the metal temperature at the critical location increased from 343° C at the start of the cycle to 1077° C at the end of heating. In all analytical cases, the minimum total strain occurred after 30 seconds of heating when the temperature at the critical location

7

was 888° C and the maximum total strain after 9 seconds of cooling or a total elapsed time of 189 seconds when the temperature was 749° C.

Predicted stress-strain hysteresis loops from the elastic analysis and the nonlinear analyses using combined and kinematic hardening models are compared in figure 6(a). These results indicate that the total strain range was not appreciably affected by the choice of constitutive model or type of stress-strain data and that an elastic analysis was adequate for the computation of the total strain range. The major differences between the elastic and nonlinear hysteresis loops were in the stress levels, which shifted in the tensile direction under inelastic straining with the largest peak and mean stresses obtained with the combined hardening model. A measure of the strain energy or plastic work is the area of the hysteresis loop. The widest hysteresis loop and, therefore, the most plastic work is shown by the kinematic hardening model in figure 6. There was no further plastic straining or work during or after the second cycle using the combined hardening model and, therefore the area and shape of the combined and elastic hysteresis loops in figure 6 remained about the same.

The nonlinear analysis using the isotropic hardening model gave essentially the same stress-strain solutions as were obtained with the combined model in figure 6(a) due to the use of the same monotonic stress-strain properties and the absence of plastic strain reversal during cycling. Therefore, the discussion of results for the combined hardening model is also applicable to isotropic hardening and the latter will not be discussed separately.

Figure 6(b) compares the stress-strain hysteresis loops from the nonlinear analyses using the combined hardening models with and without creep.

8

Inclusion of creep effects during the thermal transients had only a small effect on the peak and mean stresses with combined hardening, but resulted in substantially more strain energy per cycle as represented by the enclosed areas of the stress-strain hysteresis loops. Although the hysteresis loops for the combined-creep and kinematic models in figure 6 are shown as closed, there was some inelastic strain ratchetting which was relatively minor and therefore ignored in plotting the loops.

Stabilization of the stress-strain solution using the combined hardening model is shown in figure 7(a) where it is seen that there was no further plastic flow after the first 60 seconds of heating; this is an impossibility since the specimen could not fail in 38 cycles without undergoing substantial plastic strain cycling. In contrast the kinematic hardening results in figure 7(a) exhibit plastic strain reversal and ratchetting with a relatively constant plastic strain range per cycle. Figure 7(b) shows the inelastic strain response for the combined-creep case. Accounting for transient creep effects resulted in creep strain ratchetting on every cycle and smaller plastic strain changes with the combined hardening model. Only slight changes in the maximum equivalent creep strain were obtained with further cycling. However, the minimum equivalent creep strain increased, and therefore the creep strain range decreased, although at diminishing rates during cycling.

The computed strain histories at the critical location were used to predict crack initiation life based on the Strainrange Partitioning Life Prediction Method. The material life relationships for this method are defined in reference 14 for cast IN 100 alloy from isothermal fatigue and creep rupture tests. For these analyses the response from the kinematic model con-

tained only pp(tensile plasticity reversed by compressive plasticity) and from the combined-creep model was conservatively assumed to contain cc(tensile creep reversed by compressive creep) damage cycles. Crack initiation lives of approximately 1400 cycles were predicted in both cases compared to the observed life of 38 cycles. The overpredictions in life are not necessarily proof of the inadequacy of the structural analysis method since there is evidence that thermal cycling produces damage at a faster rate than comparable isothermal, strain-controlled test data used in the life prediction method.

In figure 8 analytical results using both combined and kinematic hardening models are compared against the experimental load-notch strain cycle from the benchmark notch test. Creep was not a significant factor under the continuous cycling, isothermal conditions of this test. The experimental results demonstrated that a stable load strain response occurred on the first cycle with only minor strain changes due to subsequent cycling. A plasticity analysis using the combined hardening model did not accurately represent the experimental results; it predicted, after initial loading, an elastic response with further cycling (fig. 8(a)). Another plasticity analysis using the kinematic hardening model demonstrated good agreement with the experimental results. Kinematic hardening predicted ratchetting between the first and second cycles and a stable notch strain cyclic response thereafter (fig 8(b)); except for slightly overpredicting the ratchetting, these results are consistent with the experimental notch cyclic response.

SUMMARY OF RESULTS

The results of the evaluation of inelastic constitutive models available in nonlinear, structural analysis computer programs can be summarized as follows:

1. Of the plasticity hardening models which were evaluated, the kinematic model gave a predicted stress-strain response most consistent with experimental observations. The combined (as well as the isotropic) model predicted elastic response during cycling which obviously did not agree with experimental results from both the thermal fatigue wedge and benchmark notch specimen tests. Creep effects were shown to be significant during thermal transients and failure to take them into account can affect the predicted stress-strain response.

2. Of the structural analysis parameters used in low-cycle fatigue damage models only the total strain range was relatively insensitive to the choice of inelastic constitutive model. Other parameters such as inelastic strain range, mean stress, and inelastic work were significantly affected by the constitutive model. The elastically computed maximum total strain range agreed well with that computed from the inelastic analyses. The elastic analysis was also able to determine the critical location for crack initiation and the cycle times when the total strain was maximum or minimum.

3. The life prediction analyses based on the structural analysis results using the kinematic and combined-creep models in conjunction with isothermal, strain controlled fatigue test data overpredicted the observed crack initiation life of the thermally-cycled wedge specimen.

REFERENCES

1. Hirschberg, M. H. and Halford, G. R., "Use of Strainrange Partitioning to Predict High-Temperature Low-Cycle Fatigue Life," NASA TN D-8072, 1976.

2. Bizon, P. T. and Spera, D. A., "Comparative Thermal Fatigue Resistances of Twenty-Six Nickel and Cobalt-Base Alloys," NASA TN D-8071, 1975.

3. MARC General Purpose Finite Element Analysis Program, User Manual, Vols. A and B, MARC Analysis Research Corpor., 1979.

4. Kaufman, A.," Elastic-Plastic Finite-Element Analyses of Thermally Cycled Single-Edge Wedge Specimens," NASA TP-1982, 1982.

5. Kaufman, A. and Hunt, L. E., "Elastic-Plastic Finite-Element Analyses of Thermally Cycled Double-Edge Wedge Specimens," NASA TP-1973, 1982.

6. Kaufman, A. and Gaugler, R. E., "Cyclic Structural Analyses of Air-Cooled Gas Turbine Blades and Vanes," SAE Paper No. 760918, 1976.

7. Kaufman, A. and Gaugler, R. E., Nonlinear, Three-Dimensional Finite-Element Analysis of Air-Cooled Gas Turbine Blades," NASA TP-1669, 1980.

8. Kaufman, A., "Comparison of Elastic and Elastic-Plastic Structural Analyses for Cooled Turbine Blade Airfoils," NASA TP-1679, 1980.

9. Moreno, V., "Combustor Liner Durability Analysis, " PWA-5684-19, Pratt and Whitney Aircraft Group, East Hartford, Conn., Feb. 1981. (NASA CR-165250.)

10. McKnight, R. L., Laflen J. H. and Spamer, G. T., "Turbine Blade Tip Durability Analysis, General Electric Company, Cincinnati, Ohio, Feb. 1981. (NASA*CR-165268.)

11. Domas, P. A., et al., "Benchmark Notch Test for Life Prediction," NASA CR-165571, NAS3-22522, 1981.

12. Nachtigall, A. J., "Cyclic Stress-Strain Curve Determination for D6AC Steel by Three Methods," NASA TM-73815, 1977.

13. Halford, G. R., "Cyclic Creep-Rupture Behavior of Three HighTemperature Alloys," Metaliurgical Transactions, Vol.3, No. 8, Aug. 1972, pp. 2247-2256

14. Halford, G. R. and Nachtigall, A. J., "Strainrange Partitioning Behavior of the Nickel-Base Superalloys, Rene' 80 and IN 100, "Characterization of Low Cycle High Temperature Fatigue by the Strain Range Partitioning Method,* AGARD-CP-243, Technical Editing and Reproduction Ltd., London, England, Apr. 1978, pp. 2-1, 2-14.

TABLE 1.   IN 100 ALLOY PHYSICAL PROPERTIES

Temperature, °C	Modulus of Elasticity, MN/m²	Mean Coefficient of Thermal Expansion, m/m/°C
316	193X10³	13.1X10⁻⁶
371	190	13.3
427	186	13.5
482	183	13.7
538	179	13.9
593	176	14.0
649	172	14.4
704	168	14.6
760	163	14.9
816	157	15.4
871	152	15.8
927	145	16.4
982	139	16.7
1038	133	17.5
1093	127	18.2

TABLE II.   IN100 ALLOY STRESS-STRAIN PROPERTIES

Temperature, °C	Cyclic, [i][j] $\sigma=K(\epsilon_p/.1)^n$		Monotonic, [j][k] $\sigma=C(\epsilon_p/.1)^m$	
	K	n	C	m
316	1005	.046	731	.078
427	944	.064	731	.078
538	869	.086	731	.078
649	777	.113	731	.078
760	665	.147	731	.078
871	528	.187	676	.078
982	361	.236	255	.146
1093	157	.297	173	.146

[i] Locus of cyclic curve tips (fig. 2)
[j] Stress (σ) in MPa, plastic strain (ϵ_p) in percent
[k] Not applicable for ϵ_p less than 0.02 percent

TABLE III.   IN 100 Alloy CREEP PROPERTIES

Temperature, °C	Creep rate, %/min., [l] $\dot{\epsilon}_{cp}=A(\sigma/6.895)^m(t)^n$		
	A	m	n
760	.00062	0.717	-0.881
871	.00012	1.709	-0.736
982	.00010	2.172	-0.654
1093	.00058	2.103	-0.634

[l] Stress (σ) in MPa, time (t) in minutes
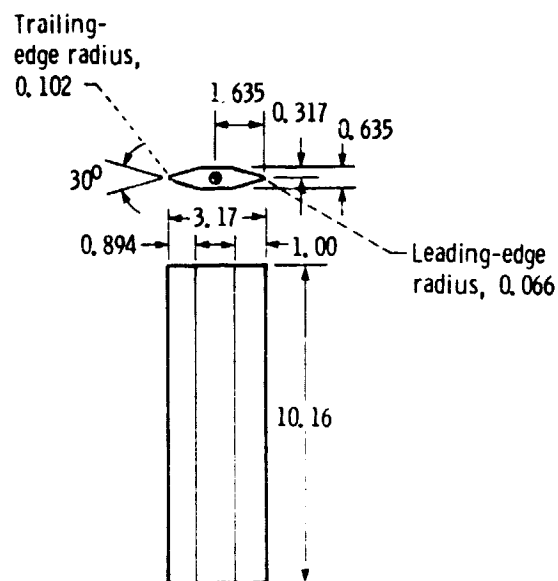
Figure 1. - Double-edge wedge. (All linear dimensions in centimeters.)
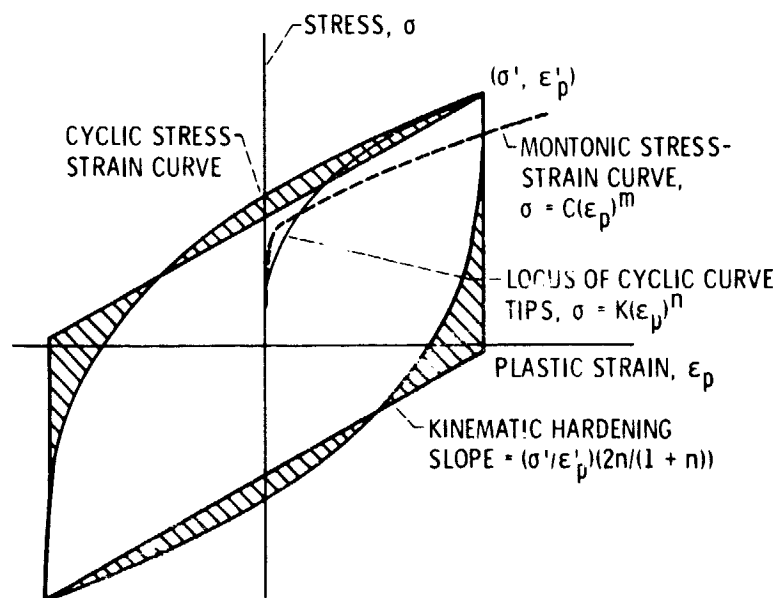

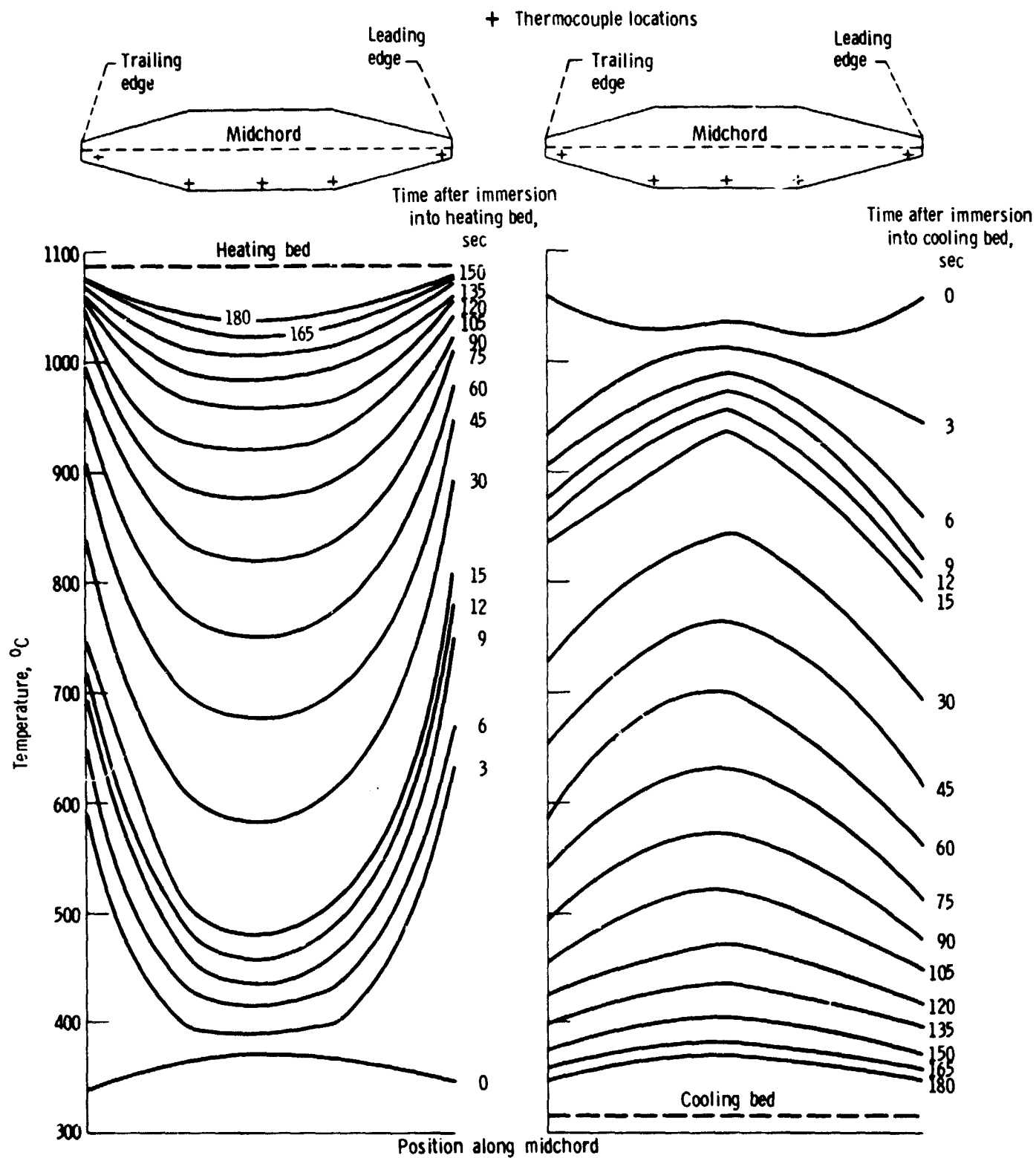Figure 2. - Representation of stress-strain curves.

Figure 3. - Temperature of midchord at midspan at various times after immersion into fluidized beds.
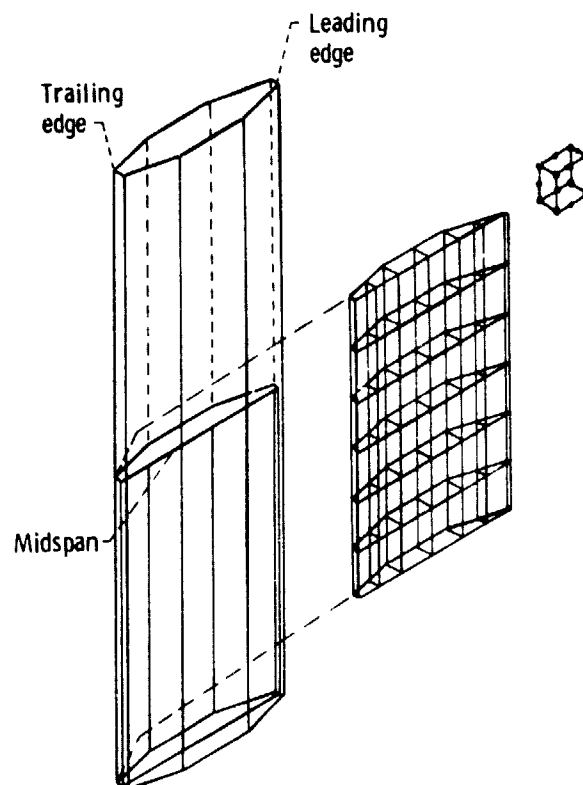
Figure 4. – Model and typical element used for MARC
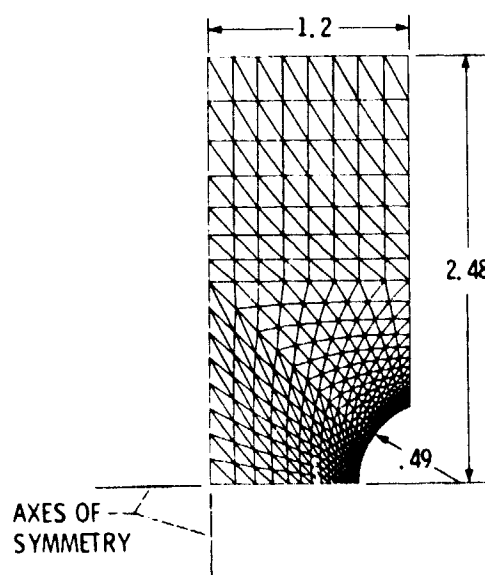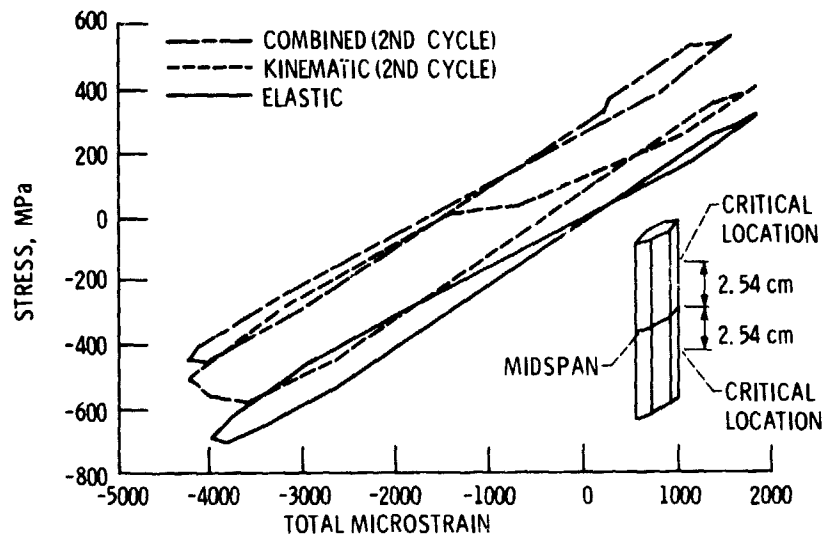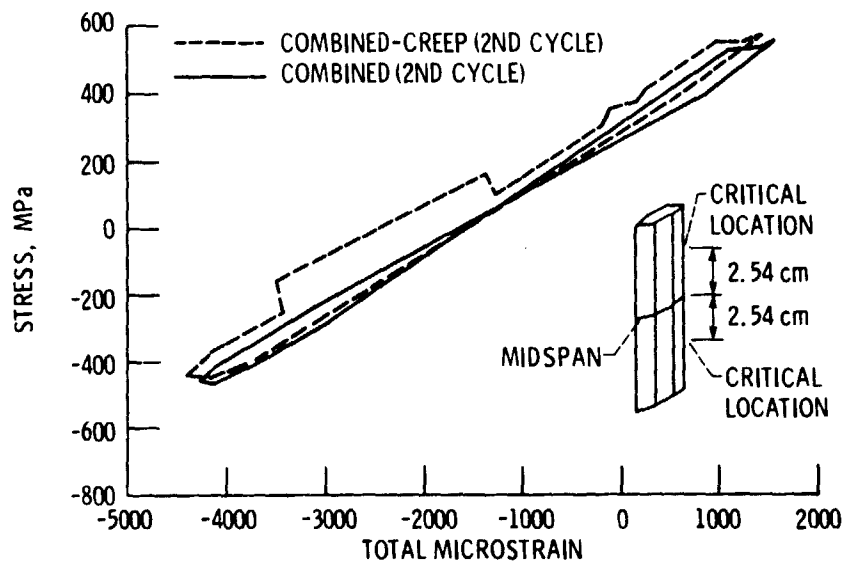analysis with coordinate convention.

Figure 5. – Benchmark notch specimen finite
element model (all dimensions in cm).

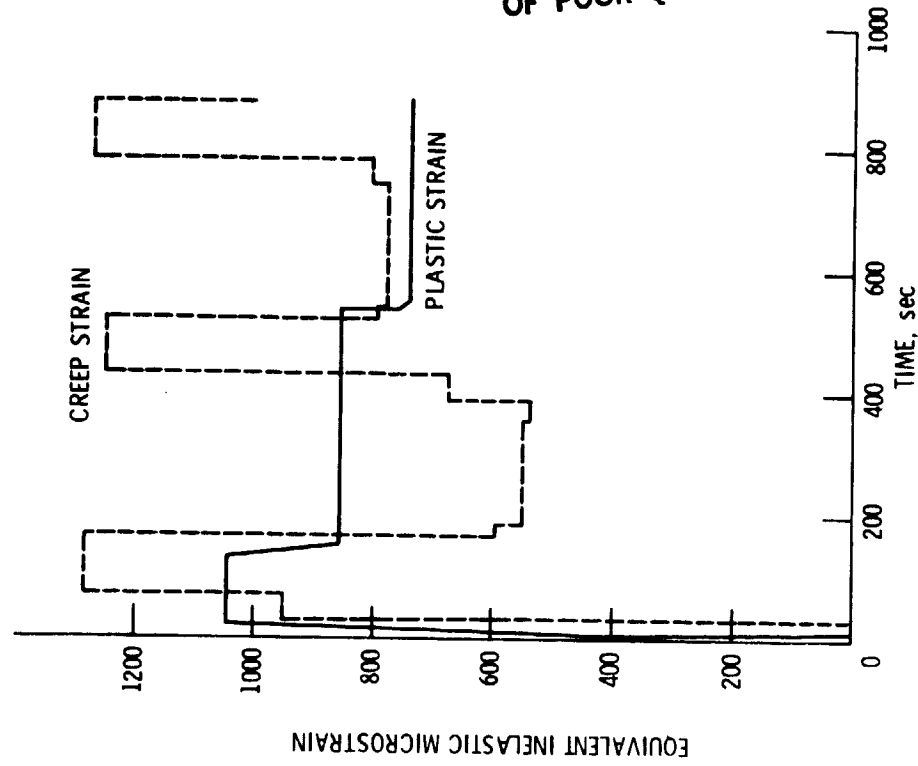(a) Comparison of combined, kinematic models and elastic results.

Figure 6. – Effect of inelastic constitutive model on stress-strain response of wedge specimen (critical location).

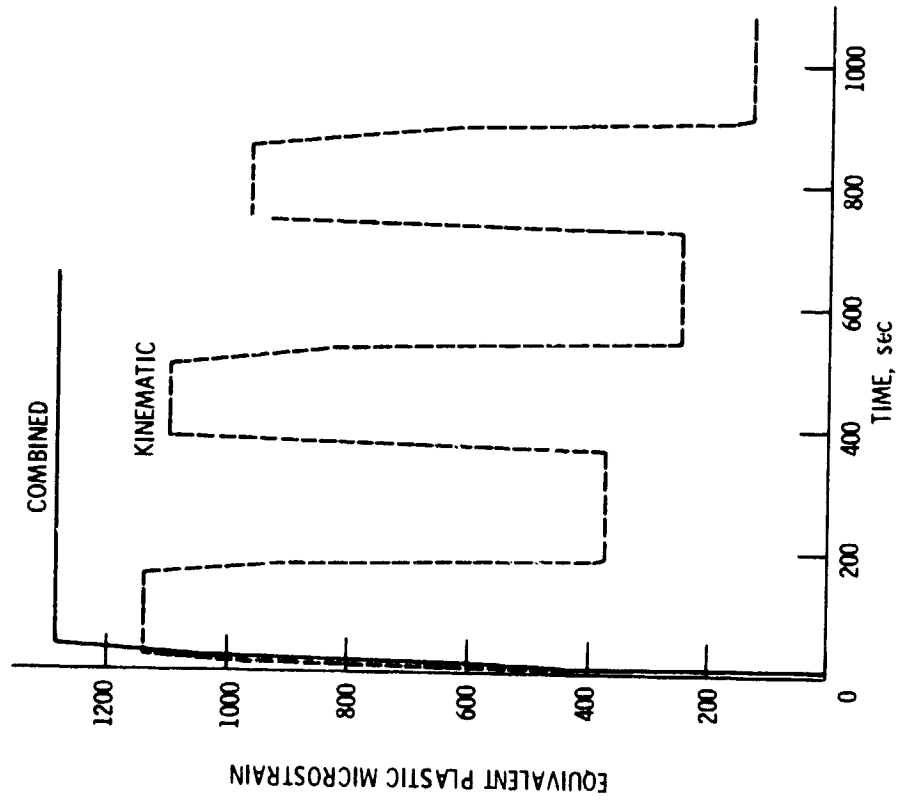(b) Comparison of combined and combined-creep models.

Figure 6. – Concluded.

CREEP STRAIN

PLASTIC STRAIN

EQUIVALENT INELASTIC MICROSTRAIN

TIME, sec

(b) Combined-creep model.

Figure 7. - Concluded.

COMBINED

KINEMATIC

EQUIVALENT PLASTIC MICROSTRAIN

TIME, sec
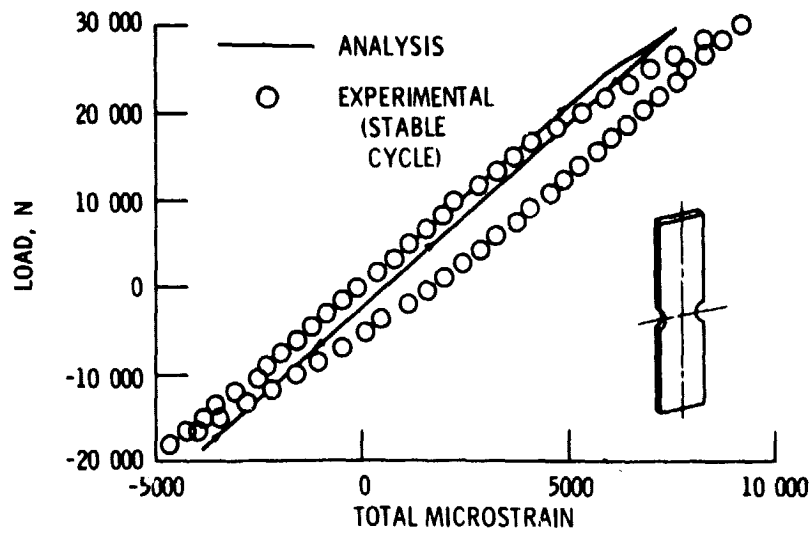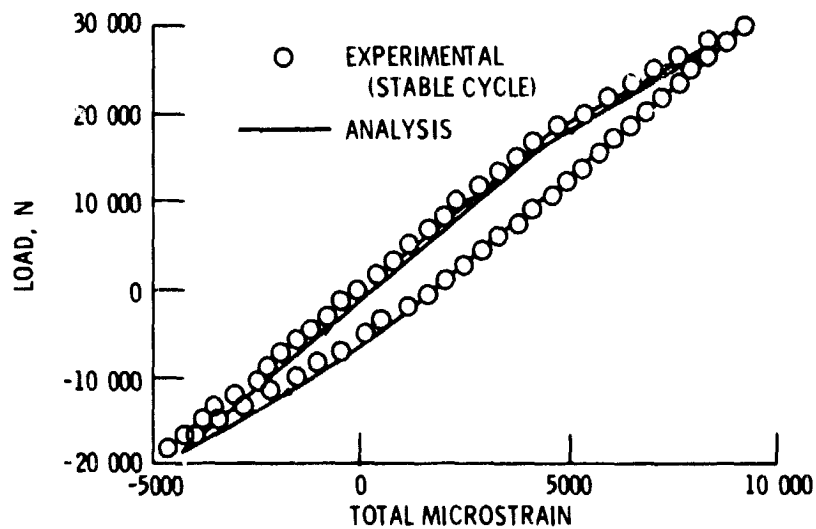
(a) Combined and kinematic models.

Figure 7. - Inelastic strain response at critical location of wedge specimen.

(a) Combined model.

Figure 8. - Comparison of benchmark notch specimen experimental and analytical results.

(b) Kinematic model.

Figure 8. - Concluded.